Inverse methods in aeroacoustic three-dimensional volumetric noise source localization

G. Battista [1], **P. Chiariotti** [1], **M. Martarelli** [2], **P. Castellini** [1]
[1] Università Politecnica delle Marche, DIISM,
Via Brecce Bianche, 60131, Ancona, Italy
e-mail: **g.battista@pm.univpm.it**

[2] Università degli studi e-Campus, Novedrate (CO), Italy

Abstract
Acoustic source mapping with microphone arrays usually involves the implicit assumption that sources are situated on the surface where the calculation points are located. However, in some application, such as aeroacoustic source localization, this assumption may produce misleading results. This paper describes the use of inverse methods in the context of aeroacoustic volumetric source imaging. A comparative investigation in exploiting a single planar array or multiple planar arrays, observing noise sources from different directions, is performed. Moreover, since aeroacoustic data are often spoiled by noise and different sources of quite different strengths are present, a novel use of CLEAN-SC as pre-processing step for inverse methods is discussed. The simulated and experimental results presented in the paper refer to a Counter Rotating Open Rotor installed on a 1/7th scale aircraft model placed in a large Low Speed Wind Tunnel.

1 Introduction

Aeroacoustic measurements are usually performed using phased-microphone array techniques to ease the noisy source identification task. Despite their simplicity and robustness, simple beamforming algorithms, like Conventional Beamforming (CB), suffer of poor dynamics and poor spatial resolution at low frequencies, which lead to difficult interpretation of maps in case of multiple sources having different levels. In three-dimensional acoustic mapping, i.e. when a three-dimensional calculation grid is used, these limitations become even more evident. Indeed, beamformers have poor spatial resolution along the focusing direction when a single array is used, while the sidelobe level dramatically increases when multiple arrays are combined, even in presence of a single monopole. These characteristics make direct beamformers not appropriate for three-dimensional source mapping. Over the years, deconvolution techniques (e.g. DAMAS [3], CLEAN-SC [9]) of beamforming maps have been developed in order to improve results accuracy in terms of spatial resolution and quantification of source strengths. The goal of these methods is to remove the effect of array spatial response, i.e. the Point Spread Function (PSF), from the map and return the real source distribution that has generated the original map and hence pressure data measured at microphone locations. Deconvolution algorithms are the only possibility to effectively use CB for volumetric mapping [14]. On the other hand, inverse methods start from a discretization of the region of interest using a cloud of elementary sources (e.g. monopoles and dipoles) and aim to return the whole source distribution which optimally approximates pressure data at microphone locations, hence having the possibility to deal with correlated and spatially-distributed sources. In [2] Battista et al. described and compared different inverse methods for three-dimensional acoustic mapping using a single planar array, while Padois et al. [10] compared the behaviour of different acoustic mapping methods using one or two planar arrays. The aim of this work is to describe some strategies to successfully perform volumetric noise source localization in aeroacoustic appli-

cations. In particular, advantages and drawbacks in using one or two planar arrays are discussed. Moreover, a novel use of CLEAN-SC as pre-processing step to inverse approaches is presented to ease the localization task when source of different strength are present (as it might be the case, in an aeroacoustic application, when considering engine and wing noises). These aspects are discussed on data recorded on a Counter Rotating Open Rotor (CROR) installed on a 1/7th scale aircraft model. The model was tested in a large Low Speed Wind Tunnel (WT) at The Pininfarina Aerodynamic and Aeroacoustic Research Center in Turin, Italy, within the framework of the FP7 EU Clean-Sky WENEMOR (Wind tunnel tests for the Evaluation of the installation effects of Noise EMissions of an Open Rotor advanced regional aircraft) project.

2 Inverse acoustic problem and solution strategies

2.1 Acoustic direct and inverse problem formulations

In frequency domain the discrete acoustic direct problem can be described, for each frequency, by the following linear relationship:

$$\mathbf{G}\mathbf{q} = \mathbf{p} \tag{1}$$

where $\mathbf{q}$ is the vector of complex source strengths of S elementary sources in assumed positions, $\mathbf{p}$ is the vector containing the complex pressures on M receiver locations and the complex matrix $\mathbf{G}$ represents the acoustic propagation matrix. The *direct acoustic problem* identifies the problem of calculating $\mathbf{p}$ for given $\mathbf{q}$ and $\mathbf{G}$. This is a well-determined problem having a unique solution. Conversely, the calculation of $\mathbf{q}$ for given $\mathbf{G}$ and $\mathbf{p}$ describes the *inverse acoustic problem*, which results to be ill-posed in Hadamard sense, i.e. existence, uniqueness and stability of solution are not guaranteed [5]. Also the inverse problem can be expressed as linear transformation

$$\hat{\mathbf{q}} = \mathbf{T}\mathbf{p}\,. \tag{2}$$

While the direct operator $\mathbf{G}$ is well-defined, the inverse operator $\mathbf{T}$ can assume different forms depending on the approach adopted. For this reason, the estimated source coefficients $\hat{\mathbf{q}}(\mathbf{T})$ depend on the assumptions and a priori information about the source distribution. A detailed review about different inverse operators is provided by Leclere et al. in [7]. Inverse problems are generally under-determined because the number of microphones is limited by practical aspects, while the number of potential sources is often larger, in particular when dealing with three-dimensional volumetric acoustic mapping. In addition, the inversion step can be very sensitive to noise present in measurements and inaccuracy in the direct operator, therefore, a regularization procedure is required. Several strategies for finding a solution to inverse acoustic problem are present in literature. For example Generalized Inverse Beamforming (GIBF) [15] or Equivalent Source Method (ESM) [13] provide methods to obtain the source coefficient distribution solving the linear formulation.

2.2 Three-dimensional acoustic inverse problem solution strategies

In the context of volumetric mapping a good spatial resolution is requested in all directions and only few potential sources in the volume of interest contributes significantly to the sound field. For these reasons a *sparse solution* is assumed. Sparsity can be enforced by minimizing the generic L_p-norm of solution, thus having the following problem:

$$\hat{\mathbf{q}}(\eta^2, p) = \arg\min_{\mathbf{q}} \left(\|\mathbf{G}\mathbf{q} - \mathbf{p}\|_2^2 + \eta^2 \|\mathbf{q}\|_p^p \right) \tag{3}$$

where $\eta^2 \geq 0$ is the *Regularization parameter*. Sparsity is enforced minimizing for $p < 2$. This problem has no analytic solution but can be solved iteratively using the following strategy:

$$\|\mathbf{q}\|_p^p = \sum_{n=1}^{N} |q_n|^p = \sum_{n=1}^{N} w_{sp,n}^2 |q_n|^2 = \|\mathbf{W}_{sp}\mathbf{q}\|_2^2\,. \tag{4}$$

This leads to the *Iteratively Reweighted Least Squares* (IRLS) [4] algorithm, which makes use of a diagonal weighting matrix $\mathbf{W}_{sp}$ to converge to a sparse solution. Weights depend on the result of the previous iteration according to the following expression:

$$w_{sp,n}^{(it+1)} = \left| \hat{q}_n^{(it)} \right|^{\frac{p-2}{2}} \tag{5}$$

where it is the current iteration and $w_{sp,n}$ is the n-th generic diagonal element. Each iteration is a regularized least-square problem solved using the general form of *Tikhonov regularization* [16]

$$\hat{\mathbf{q}}(\eta^2, \mathbf{W}) = \arg\min_{\mathbf{q}} \left(\|\mathbf{G}\mathbf{q} - \mathbf{p}\|_2^2 + \eta^2 \|\mathbf{W}\mathbf{q}\|_2^2 \right) . \tag{6}$$

As the exponent of weights is negative for $p < 2$, division by null elements must be somehow avoided to have an invertible weighting matrix. This algorithm boils down to an iterative procedure that is a fixed-point for Eq. 3 and converges to global minimum for convex problems ($p \geq 1$) or to a global or local minimum for non-convex problem ($0 \leq p < 1$).

Tikhonov regularized solution results a particular case of a more general approach to inverse acoustic problems which has been proposed by Antoni [1]. He exploited Bayesian inference for developing a method which is able to

- identify the optimal basis functions which minimize the reconstruction error, given the topology of the specific acoustic problem;
- include *a priori* information on source distribution to better condition the problem and ease the localization task;
- provide a robust regularization criterion.

The *Bayesian Approach* (BA) encodes measurement errors in the *likelihood function* which describes the direct probability to measure certain pressures values, given the propagation model and the probability density function of measurement noise. If complex normal *prior probability density function* (pdf) for source coefficients is assumed, the Bayesian framework "mechanically" produces a regularized solution similar to the Tikhonov one. Instead, assuming a p-generalized normal distribution as prior pdf, cost function of Eq. 3 appears from BA [6]. In addition BA explicitly identifies the regularization parameter η^2 in the Noise-to-Signal Ratio and provides its estimation as *Maximum A Posteriori* estimation (MAP), selecting the value with the maximum probability of occurrence, given the measurements. The cost function to estimate η^2 provided by BA has a unique global minimum and outperform many other regularization strategies. For this reason, the regularization task in this work is fulfilled by empirical Bayesian regularization. The interested reader might refer to [12] for a deeper insight into BA.

The IRLS procedure to solve the inverse acoustic problem can be formalized with the following expression:

$$\hat{\mathbf{q}}^{(it+1)} = F\left(\hat{\mathbf{q}}^{(it)}, \mathbf{W}^{(it)}, \eta^{2\,(it)}, \mathbf{G}, \mathbf{p}, p \right) . \tag{7}$$

where the function F is given by Eq. 6. From a Bayesian point of view this method can be seen as an Expectation-Maximization algorithm which converges to MAP solution. The following algorithm is used:

1. Set the weighting matrix for the current iteration $\mathbf{W}^{(it)} = \mathbf{W}_0\, \mathbf{W}_{sp}^{(it)}$, where $\mathbf{W}_{sp}^{(1)} = \mathbf{I}$ and $\mathbf{W}_0$ is used to introduce a priori information on source distribution. Both matrices are normalized such that $\|\mathbf{W}_0\|_\infty = \|\mathbf{W}_{sp}^{(it)}\|_\infty = 1$.
2. Estimate the regularization parameter $\eta^{2\,(it)}$ for the current iteration.

3. Calculate the solution $\hat{\mathbf{q}}^{(it+1)}$ and apply a threshold to discard potential sources that do not contribute significantly to the acoustic field using the following criterion

$$10\log_{10}\left(\frac{\hat{\mathbf{q}}^{(it+1)}}{\|\hat{\mathbf{q}}^{(it+1)}\|_\infty}\right) < THR_{dB}\,. \tag{8}$$

4. Calculate $\mathbf{W}_{sp}^{(it+1)}$ using Eq. 5.

5. Evaluate a convergence criterion; if not fulfilled go back to step 1, otherwise stop the iterative procedure.

This approach returns a sparse solution for the inverse acoustic problem. A priori information can be used to penalize region where is less likely to find sources. For example Padois et al. [11] proposed to use CB map for similar purposes. In fact, CB map is rough and smooth but it provides robust estimation of source location. The discard of sources is done both for avoiding the division by zero in calculation of weights and for speeding up the algorithm. The threshold used in this work is $THR_{dB} = -100$ dB. In [2] a convergence criterion is proposed:

$$\varepsilon^{(it)} = 10\log 10\left(MSR - \left|\frac{\mathrm{d}(MSR)}{\mathrm{d}(it)}\right| - \left|\frac{\mathrm{d}^2(MSR)}{\mathrm{d}(it)^2}\right|\right) \quad , \quad MSR = \left\langle\left|\hat{q}_n^{(it)}/\hat{q}_n^{(it-1)}\right|\right\rangle \tag{9}$$

where MSR stands for *Mean Source Ratio* and the operator $\langle\cdot\rangle$ refers to the spatial average. This criterion can be evaluated only for $it > 2$ (given the second derivative term) and requires solution variation to be small over three last iterations. The algorithm stops when $\varepsilon^{(it)} \geq -0.1$ dB. Elements of the $\mathbf{G}$ matrix are calculated using the following pressure-to-pressure acoustic transfer function formulation

$$G_{mn} = \frac{r_{0n}}{r_{mn}} e^{-\mathrm{j}k(r_{mn}-r_{0n})} \tag{10}$$

which returns the acoustic pressure at microphone location m depending on sound pressure at reference point "0" caused by the monopole source at location n. The terms r_{mn} correspond to geometric distances in case of free-field propagation. Instead, in presence of flow, these terms are calculated as virtual distances corresponding to the actual travelling time for a given flow field and speed of sound. In this paper, the assumption of an uniform flow in wind tunnel is made, thus leading to the following expression for r_{mn}:

$$r_{mn} = \frac{\|\mathbf{r}_n - \mathbf{r}_m\|_2}{-C_{mn} + \sqrt{C_{mn}^2 - M_a^2 + 1}} \quad , \quad C_{mn} = (\mathbf{r}_n - \mathbf{r}_m)\cdot\hat{\mathbf{f}}\, M_a \tag{11}$$

where $\hat{\mathbf{f}}$ is the flow direction and M_a is the Mach number. A critical aspect for three-dimensional inverse acoustic mapping is to balance the energy needed by sources to induce a certain pressure on microphone locations, otherwise the farthest sources would be easily excluded in the norm minimization process. The acoustic propagator in Eq. 10 manages to achieve this task without any weighting strategy required.

2.3 Pressure data

In aeroacoustic measurements, pressure data is generally processed in frequency domain to obtain the CSM $\mathbf{P}$, given the random nature of aeroacoustic noise. Since the CSM is Hermitian and non-negative definite, it can be decomposed as

$$\mathbf{P} = \mathbf{E}_{vec}\,\mathbf{E}_{val}\,\mathbf{E}_{vec}^H\,, \tag{12}$$

where $\mathbf{E}_{vec}$ is a unitary matrix of M orthonormal eigenvectors and $\mathbf{E}_{val}$ is a diagonal matrix containing the corresponding eigenvalues (the superscript ^{H} stands for the conjugate transpose). It is possible to define the eigenmode $\mathbf{e}_i$ as the eigenvector including its amplitude

$$\mathbf{e}_i = \sqrt{e_{val,i}}\,\mathbf{e}_{vec,i} \qquad i = 1,\ldots,M \tag{13}$$

where $\mathbf{e}_{vec,i}$ is the $i\text{-}th$ eigenvector and $e_{val,i}$ is the corresponding eigenvalue. Under the constraint of orthogonality, each eigenvector represents a coherent signal across the microphones. For this reason Suzuki proposes to solve an inverse problem for each eigenmode [15]:

$$\mathbf{G}\mathbf{q}_i = \mathbf{e}_i \qquad i = 1, \ldots, M_0 \tag{14}$$

where M_0 is the number of relevant eigenmodes. When dealing with aeroacoustic measurements, the trend of eigenvalues of CSM is typically smooth, thus making difficult to properly set M_0 for each frequency.

A different method to extract source components from CSM is to exploit the CLEAN-SC procedure described by Sijtsma [9]. This iterative procedure extracts the coherent source components exploiting the fact that side lobes of a single source CB map are spatially coherent with their main lobe. The concept of spatial source coherence is described in [8]. At the end of CLEAN-SC procedure, where a loop gain $\varphi = 1$ is used, the source components $\mathbf{c}_i$ are calculated similarly to the eigenmodes as

$$\mathbf{c}_i = \sqrt{P_{max}^{(i-1)}}\,\mathbf{h}^{(i)} \qquad i = 1, \ldots, IT \tag{15}$$

where IT is the number of iterations for each frequency. Indeed, if the source components are considered as in an eigenmode decomposition approach, the inverse problem can be modelled as

$$\mathbf{G}\mathbf{q}_i = \mathbf{c}_i \qquad i = 1, \ldots, M_0\,. \tag{16}$$

In this case the number of relevant components M_0 for each frequency is given directly by the number of iterations IT, which corresponds to the number of extracted components. Independently of decomposition used, a full map can be obtained summing all contributes. This approach can therefore be used as a preprocessing step to the inverse calculation phase, thus giving the possibility to spatially separate sources of very different strengths. To the authors' knowledge, this is the first time CLEAN-SC is used for such a purpose.

3 Application results

3.1 Reference set-up

The test program was conducted at the Pininfarina Aerodynamic and Aeroacoustic Research Center in Turin, Italy within the EU WENEMOR project. Pininfarina's facility contains a test section of 8 m $\times$ 9.6 m $\times$ 4.2 m (see Figure 1(a)). The wind tunnel was specifically acoustically treated in order to reduce reverberation and background noise. Two planar microphone arrays were installed at Pininfarina Wind Tunnel (WT), as depicted in Figure 1(b): a 78 microphone wheel array (3 m diameter) placed at the ceiling of the WT at a distance of 2.5 m from the model axis and a 66 microphone half-wheel array (3 m diameter) located broadside, parallel to the axis of the open rotor and 4.2 m far from the longitudinal axis of the model. Signals were synchronously sampled at a sample rate of 32,768 Hz for a total observation length of 10 s. Time data has been processed to estimate the CSM using Welch's method (block size: 1024 samples, overlap: 50%, window: Hanning).

The CROR tested featured two rotors of 12 blades each. Both left and right engines of the aircraft model were driven from a single power supply and controlled by dedicated control systems (one per motor). Strouhal number scaling was performed to represent flight conditions of the full scale aircraft. Different design configurations of the model were tested during the whole test campaign (different tails, CROR in pusher and tractor configuration, different distances of the CRORs with respect to the model fuselage, etc.) at different flow speeds and angles of attack. Angle of attacks (AoA) differed also with respect to the take-off or approach model configuration. However, all the results discussed in this paper refer to the T-tailed model, in approach condition with CRORs in pusher configuration for AoA = 8 deg and flow speed of 28 m/s. The flow direction is considered to be the X positive axis of the coordinate system represented in Figure 1(b).

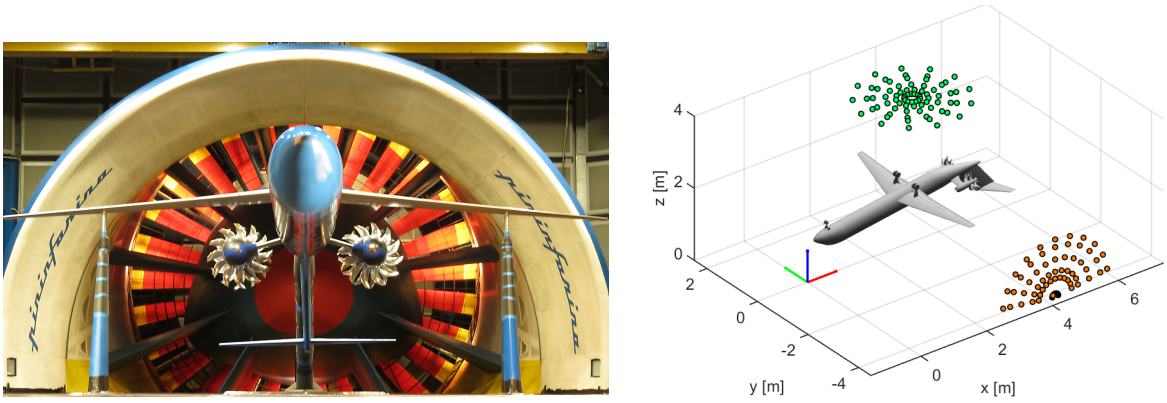

(a) (b)

Figure 1: (a) Test set-up in Pininfarina WT (front view of the aircraft model). (b) Microphone array layout with respect to WT and aircraft model (green dots: top wheel array, orange dots: side half-wheel array)

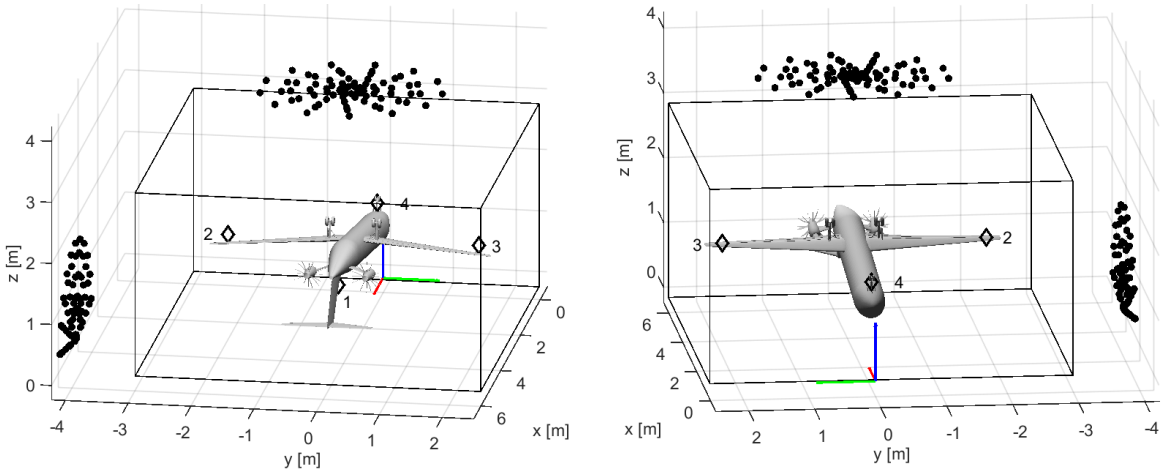

(a) (b)

Figure 2: Position of simulated sources (black diamonds) with respect to the aircraft model. The black dots represent microphone locations of the two arrays - (a) Rear view. (b) Front view.

3.2 Simulated data

Before analysing the experimental data recorded, some simulated test cases are presented to better understand performance of methods in terms of source separation capability, dynamics and robustness in case of different level of background noise. Each simulated test case consists of four monopoles emitting uncorrelated white noise and located in the four spots depicted in Figure 2. Monopoles level and coordinates are chosen in order to simulate typical sources of noise expected in a real setup. Source 1 is the loudest (1 Pa rms at 1 m distance) and represents the CROR noise, sources 2 and 3 represent the wing tip noise and are 10 dB weaker than source 1, source 4 is positioned on the front landing gear and is 20 dB weaker than source 1. During measurement campaign, time signals of real WT noise were acquired by the arrays without the model in the test section at flow speed of 28 m/s. These signals have been used as background noise (BGN), in the synthesis of simulated signals, to obtain more realistic simulations. The simulated total pressure $p_{tot,m}(t)$ on each microphone is obtained as follows

$$p_{tot,m}(t) = p_{sig,m}(t) + G \cdot p_{bgn,m}(t) \qquad m = 1, \ldots, M \tag{17}$$

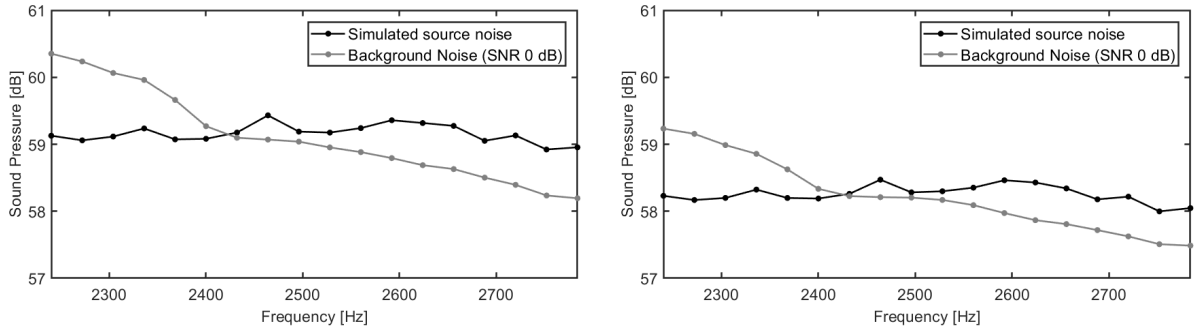

(a) (b)

Figure 3: Average microphone auto-spectra - (a) Top array, (b) Side and top arrays

where $p_{sig,m}(t)$ is the contribution of all simulated sources on each microphone and $p_{bgn,m}(t)$ is the real WT noise recorded by each m-th microphone. The desired Signal-to-Noise Ratio (SNR) is obtained by setting the proper gain G and has been calculated using microphone auto-spectra, averaged over all microphones, respectively of simulated and real WT noise signals. Once selected the band of interest, the overall band power P_{sig} and P_{bgn} are estimated and G is calculated as

$$G = \sqrt{\frac{P_{sig}}{P_{bgn}}} 10^{(-\mathrm{SNR}_{dB}/20)} \tag{18}$$

where SNR_{dB} is the target SNR, expressed in dB. In this way data produced have an overall SNR $= P_{sig}/P_{bgn}$ for the whole band of interest. Two different test cases are shown in this section: noise-free and SNR $= 0$ dB. Figure 3 shows the average microphone auto-spectrum induced by simulated source noise compared with average microphone auto-spectrum of background noise added for the noisy test case. All acoustic maps reported refers to one-third octave band at 2500 Hz.

The volume of interest, depicted in Figure 2, contains the whole model and it is discretized with a regular grid of monopoles using a step of 0.06 m, thus having 464,508 potential sources in the volume. Maximum solution sparsity is obtained by setting $p = 0$. Both eigenmodes and CLEAN-SC decomposition of CSM are used to map noise sources and then compared in terms of localization and robustness to noise. All CLEAN-SC extracted components are analysed while the number of relevant eigenmodes is set to $M_0 = 20$. The inverse method described in the previous section is applied without any change when single or multiple array are utilized. In addition, it is also tested if the use of CB map of single components as a priori information $\mathbf{W}_0$ can improve results. All maps report the sound pressure level at the reference point, that is the origin of the coordinate system and are represented using a dynamic range of 50 dB.

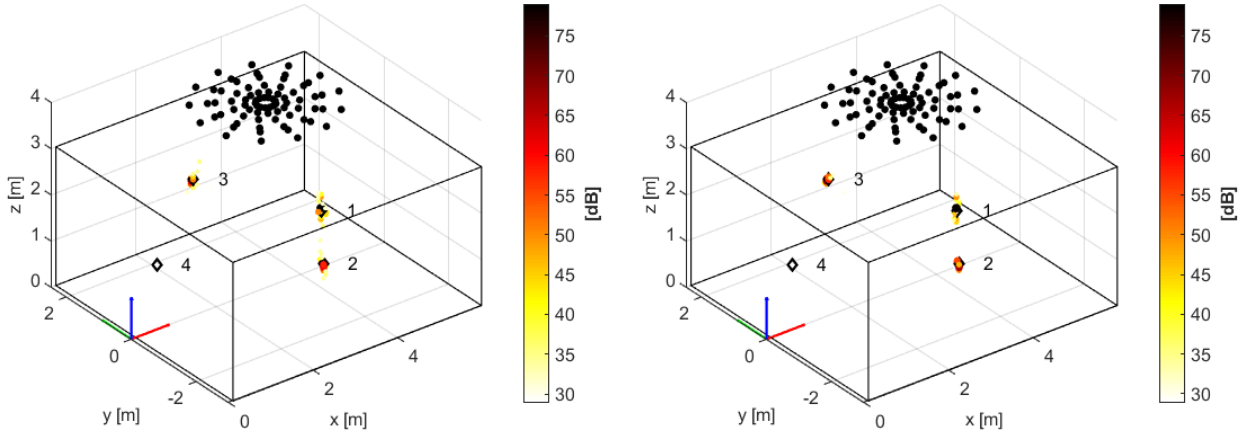

(a) (b)

Figure 4: Noise-free simulation, top array - (a) CLEAN-SC Components, (b) Eigenmodes

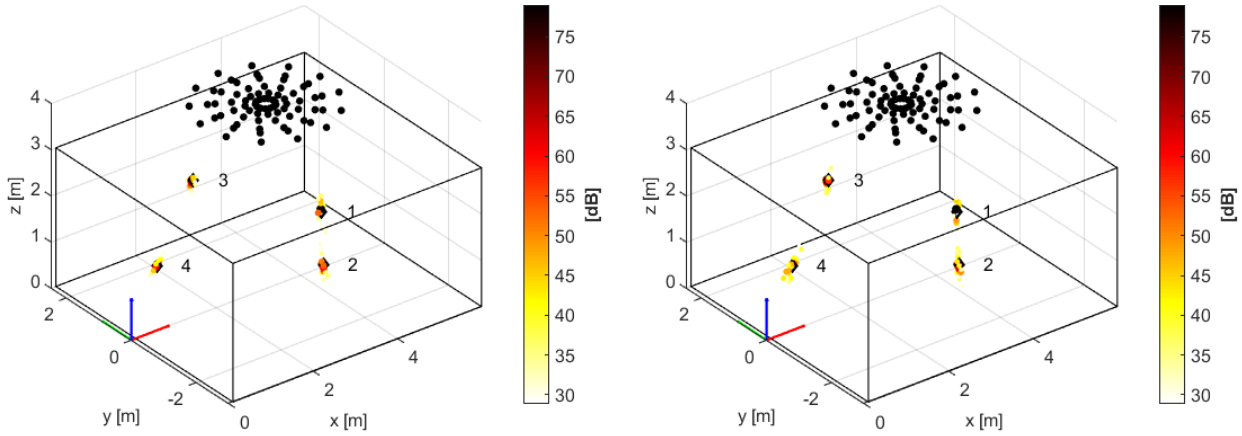

(a) (b)

Figure 5: Noise-free simulation, top array with CB map as a priori information - (a) CLEAN-SC Components, (b) Eigenmodes

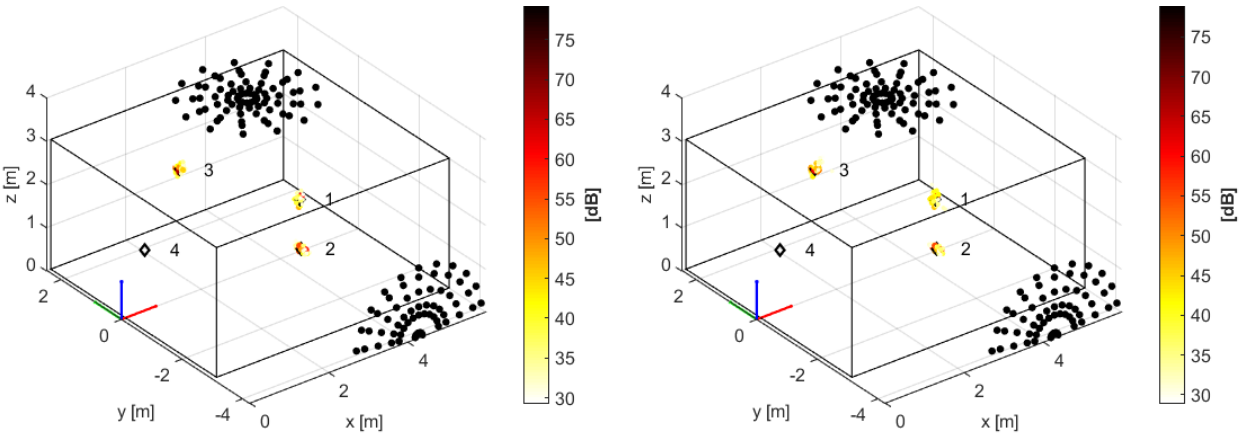

(a) (b)

Figure 6: Noise-free simulation, side and top arrays - (a) CLEAN-SC Components, (b) Eigenmodes

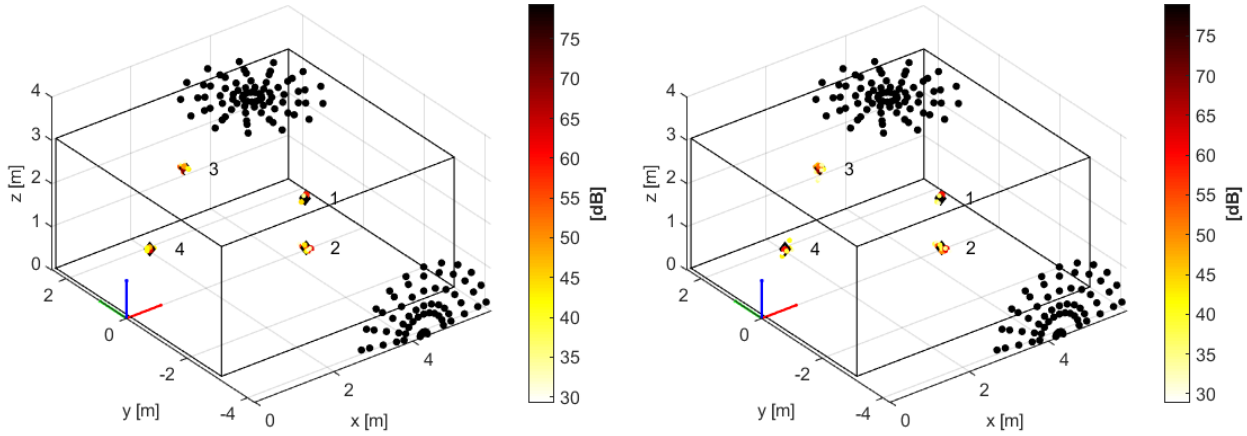

(a) (b)

Figure 7: Noise-free simulation, side and top arrays with CB map as a priori information - (a) CLEAN-SC Components, (b) Eigenmodes

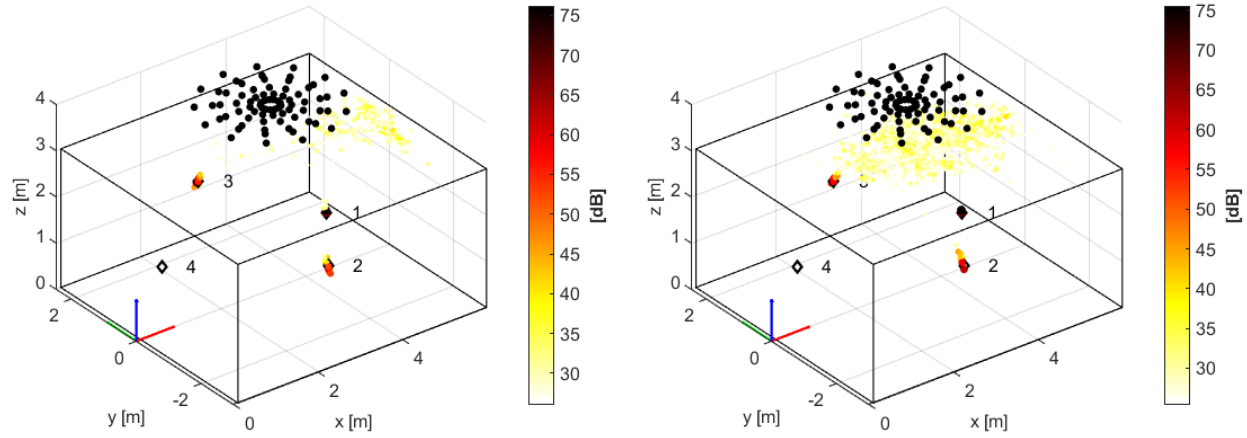

(a) (b)

Figure 8: Simulation with SNR $= 0$ dB, top array - (a) CLEAN-SC Components, (b) Eigenmodes

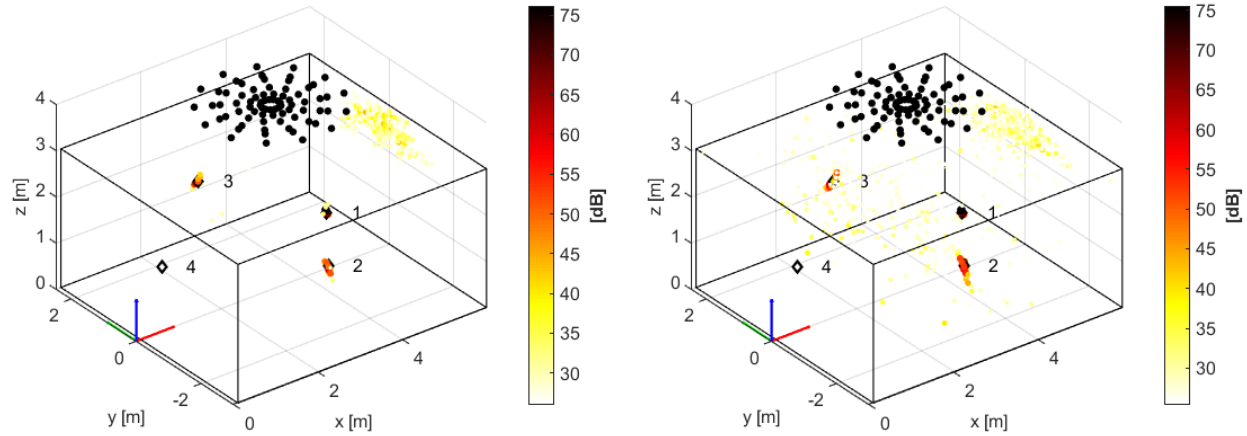

(a) (b)

Figure 9: Simulation with SNR $= 0$ dB, top array with CB map as a priori information - (a) CLEAN-SC Components, (b) Eigenmodes

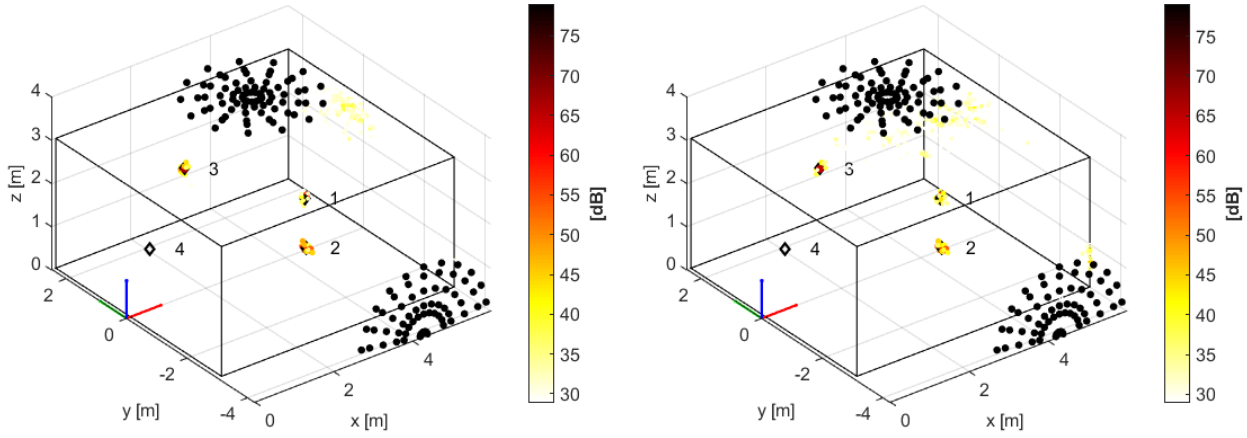

(a) (b)

Figure 10: Simulation with SNR = 0 dB, side and top arrays - (a) CLEAN-SC Components, (b) Eigenmodes

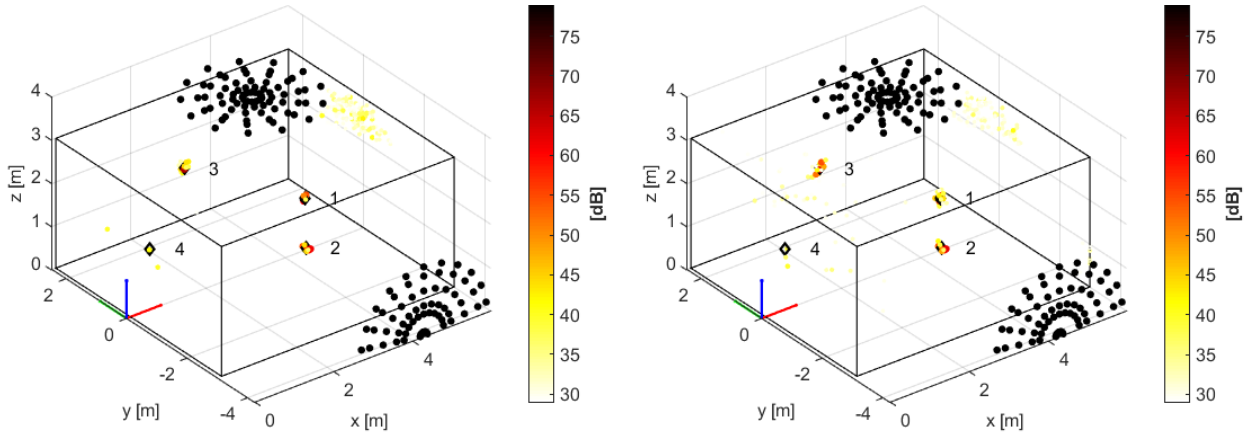

(a) (b)

Figure 11: Simulation with SNR = 0 dB, side and top arrays with CB map as a priori information - (a) CLEAN-SC Components, (b) Eigenmodes

These results show how it is possible to properly combine different strategies and arrays to have maps with high accuracy and dynamics even in presence of strong noise. Indeed, a priori information introduced make possible to reconstruct even the weakest source, while the use of the second array increases localization accuracy and the capability of suppressing noise and artefacts.

3.3 Experimental data

The band analysed is the same of simulated test cases. The number of relevant eigenmodes is empirically set to $M_0 = 30$ because otherwise noise spoils excessively the components. All CLEAN-SC components are processed resulting to be $M_0 < 30$ for each frequency within the band analysed. The volume of interest and its discretization are the same of the simulated test cases. Figures from 12 to 15 show results for the test case with the CRORs switched-on. Figures from 16 to 19 show the acoustic maps with the CRORs switched-off. All data are represented using a dynamic range of 30 dB.

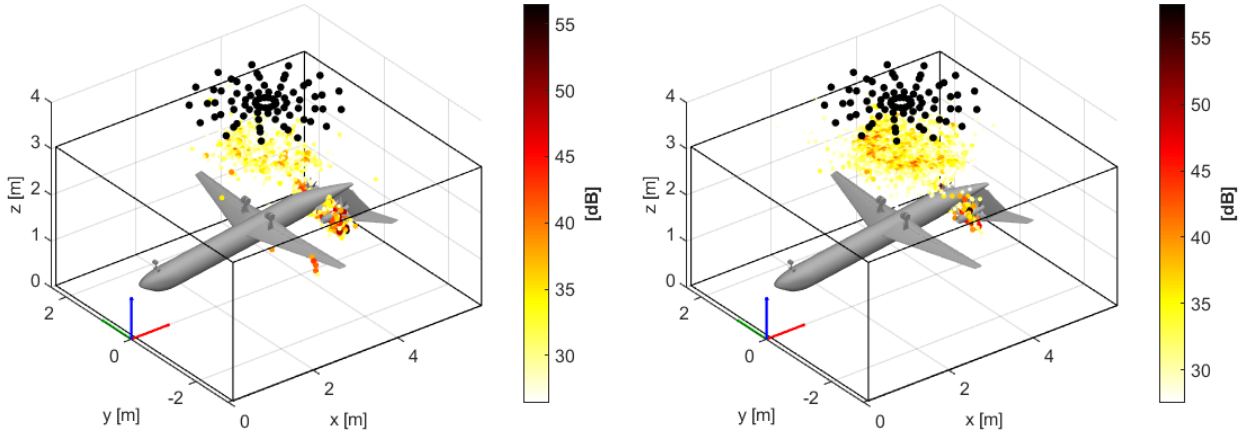

(a) (b)

Figure 12: CROR turned-on, top array - (a) CLEAN-SC Components, (b) Eigenmodes

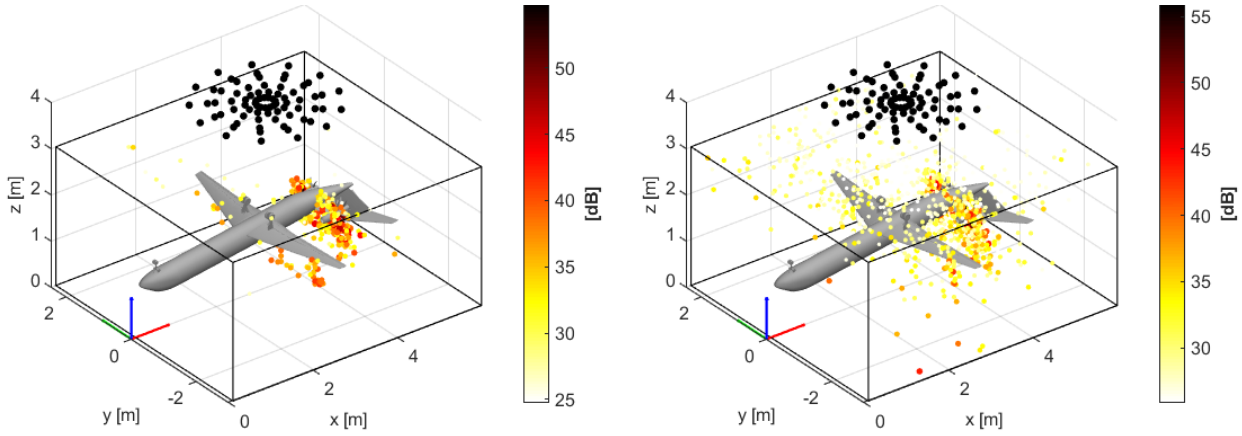

(a) (b)

Figure 13: CROR turned-on, top array with CB map as a priori information - (a) CLEAN-SC Components, (b) Eigenmodes

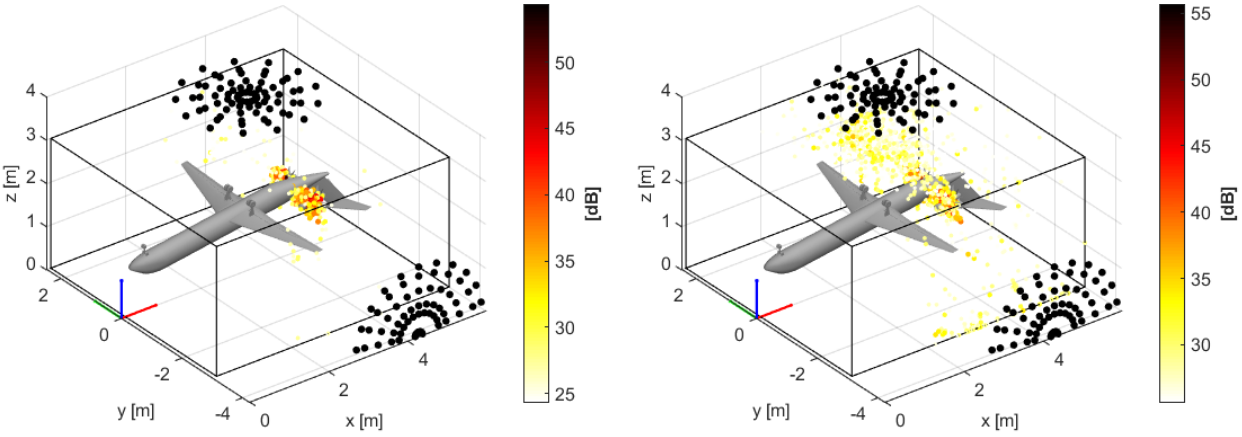

(a) (b)

Figure 14: CROR turned-on, side and top array - (a) CLEAN-SC Components, (b) Eigenmodes

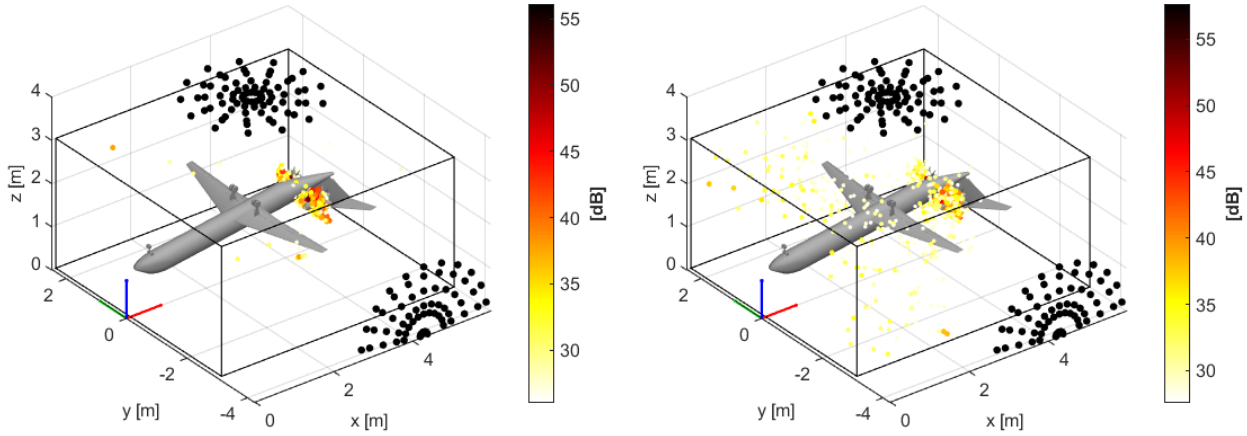

(a) (b)

Figure 15: CROR turned-on, side and top array with CB map as a priori information - (a) CLEAN-SC Components, (b) Eigenmodes

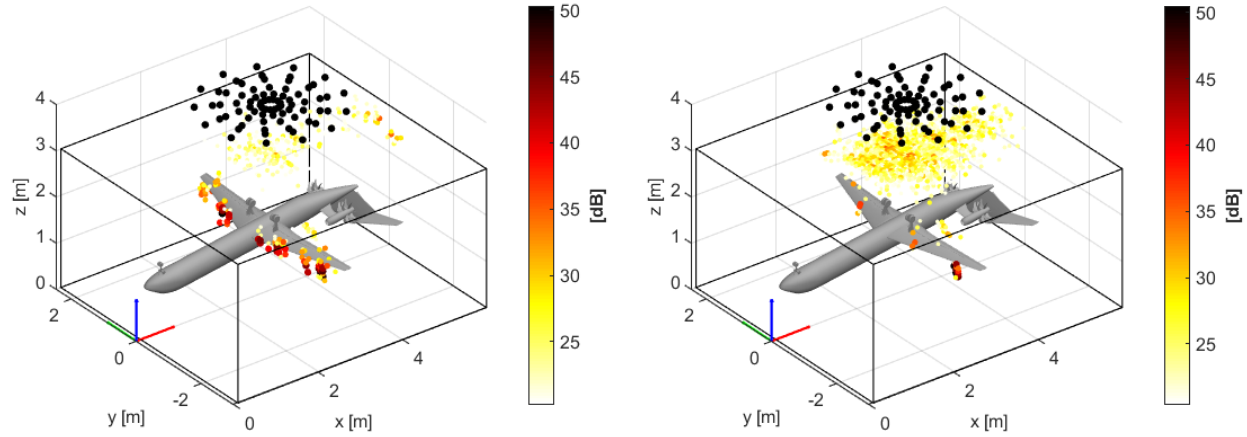

(a) (b)

Figure 16: CROR turned-off, top array - (a) CLEAN-SC Components, (b) Eigenmodes

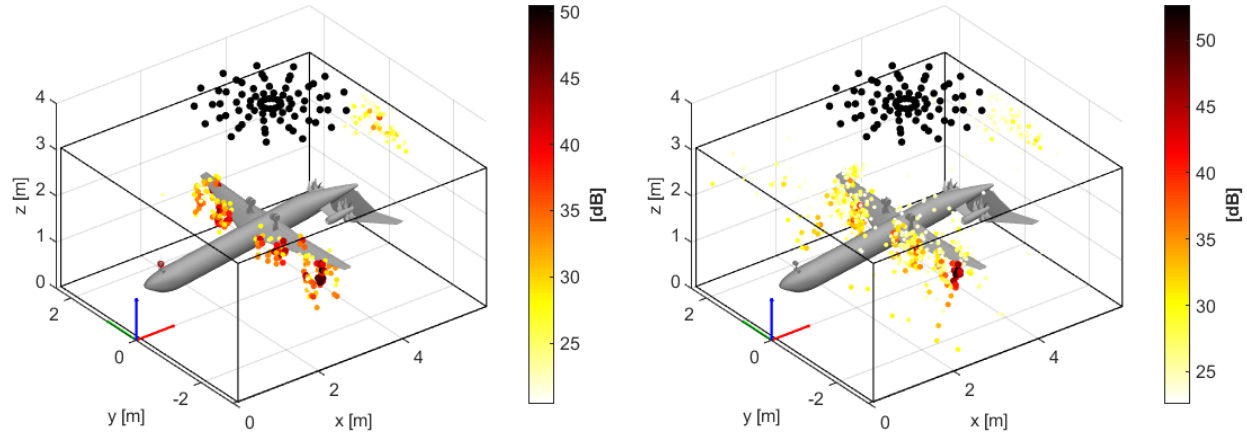

(a) (b)

Figure 17: CROR turned-off, top array with CB map as a priori information - (a) CLEAN-SC Components, (b) Eigenmodes

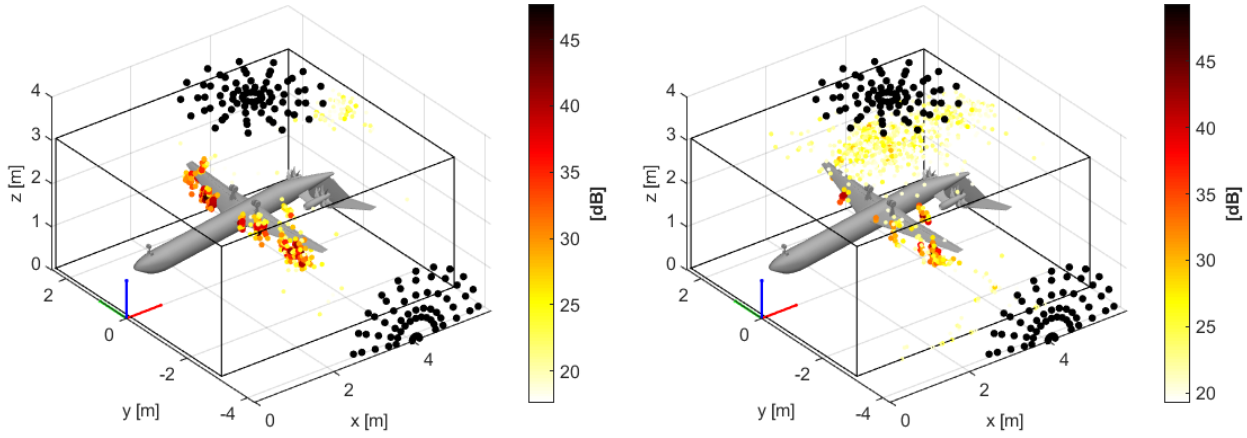

(a) (b)

Figure 18: CROR turned-off, side and top array - (a) CLEAN-SC Components, (b) Eigenmodes

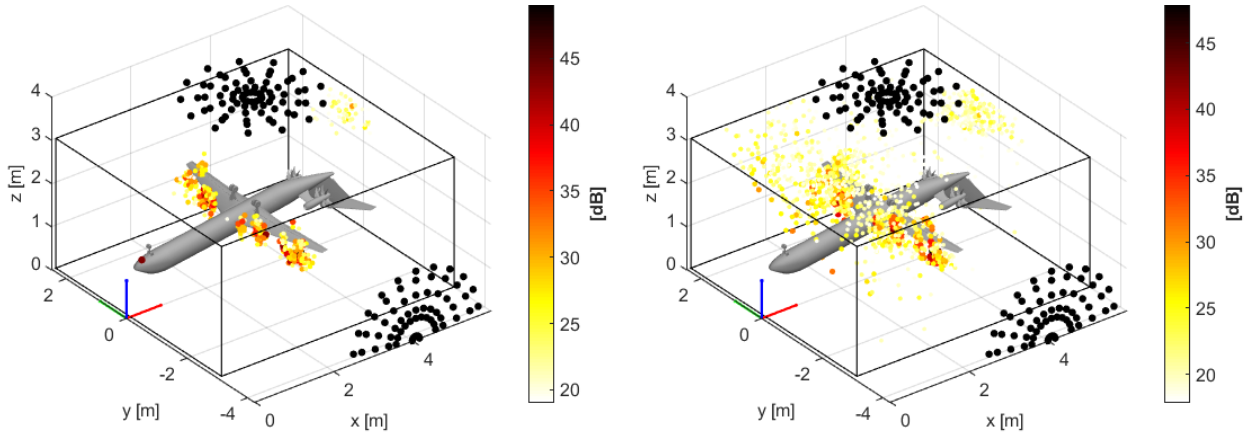

(a) (b)

Figure 19: CROR turned-off, side and top array with CB map as a priori information - (a) CLEAN-SC Components, (b) Eigenmodes

The presence of CRORs noise makes difficult the task of locating weaker noise sources. The use of two arrays gives an improvement in the localization of rotors noise, while it brings no advantage in the aeroacoustic source localization. Indeed, only in Figure 13(a), some aeroacoustic sources are clearly visible in addition to the CROR sources. When CRORs are turned-off, some sources close to the wings, that might hint to wing tip noise, starts to appear on the maps, even if the background noise remains the same. In some of the results presented for the single-array case, it is clearly visible that a lot of energy is located close to the array. When this phenomenon occurs, it means that the regularization process fails due to the high level of noise and the severe under-determination of the problem. Moreover, these results remark the difference between CLEAN-SC components and eigenmodes. Indeed the former usually give less artefacts in the maps due to lower level of noise in the CSM components.

4 Conclusions

This work described how to exploit inverse methods in the context of volumetric mapping targeted to aeroacoustic applications. The problem has been faced both from the point of view of the algorithm and from the possible choice to use multiple planar arrays on orthogonal planes. The main issues that have been faced are:

- severely under-determined inverse problems due to the great number of potential sources in volumes,
- high level of noise present in aeroacoustic data,
- sources having large difference in terms of strengths.

The first issue entails the ill-posedness and ill-conditioning of the problem. These two characteristics are addressed by using an IRLS algorithm that enforces sparsity of solution and exploits BA as regularization strategy. The other two issues have been faced, in this paper, by performing a decomposition of the microphone CSM, which makes it possible to separate source components from noise, and by exploiting the a priori information on source distribution provided by CB. With this in mind, a novel approach that uses CLEAN-SC as pre-processing step to inverse method has been presented. The novel approach generally outperforms the classic eigenmodes decomposition typically adopted, with the further advantage of providing the number of relevant components in the pressure CSM. Moreover, the introduction of CB map for each component as a priori information in the inverse problem makes possible to correctly reconstruct even sources 20 dB weaker than the principal one.

Results from both simulated and experimental data demonstrated that is possible to use a single planar array to map aeroacoustic noise sources with fair accuracy. The use of a second array is suggested when localization accuracy is crucial. However, the downside of combining multiple arrays looking at the acoustic scene from different point of view, is that one of them may not detect enough signal from some sources acting in the scenario (e.g. due to masking effect of the target or excessive source directivity) thus deteriorating the reconstruction of these sources.

Independently on the use of one or two arrays, results showed that the algorithm and the strategies described in this work can lead to accurate volumetric source localization even in presence of strong background noise.

Acknowledgements

The research leading to these experimental data has received funding from the European Unions Seventh Framework Programme (FP7/2007-2013) for the Clean Sky Joint Technology Initiative under grant agreements n^{o} 278419 (WENEMOR). Authors kindly acknowledge all the partners.

References

[1] Jérôme Antoni. A bayesian approach to sound source reconstruction: Optimal basis, regularization, and focusing. *The Journal of the Acoustical Society of America*, 131(4):2873–2890, apr 2012.

[2] Gianmarco Battista, Paolo Chiariotti, Gert Herold, Ennes Sarradj, and Paolo Castellini. Inverse methods for three-dimensional acoustic mapping with a single planar array. In *Proceedings of the 7th Berlin Beamforming Conference*, 2018.

[3] T. F. Brooks and W. M. Humphreys, Jr. A Deconvolution Approach for the Mapping of Acoustic Sources (DAMAS) Determined from Phased Microphone Arrays. In *10th AIAA/CEAS Aeroacoustics Conference*, 2004.

[4] Rick Chartrand and Wotao Yin. Iteratively reweighted algorithms for compressive sensing. In *2008 IEEE International Conference on Acoustics, Speech and Signal Processing*. IEEE, mar 2008.

[5] Jacques Hadamard. Sur les problèmes aux dérivés partielles et leur signification physique. *Princeton University Bulletin*, 13:49–52, 1902.

[6] Q. Leclere, Antonio A. Pereira, and Jérôme Antoni. Une approche bayésienne de la parcimonie pour l'identification de sources acoustiques. In *Congrès Français d'Acoustique*, pages –, Poitiers, France, 2014.

[7] Quentin Leclère, Antonio Pereira, Christophe Bailly, Jerome Antoni, and Christophe Picard. A unified formalism for acoustic imaging techniques: illustrations in the frame of a didactic numerical benchmark. In *Proceedings on CD of the 6th Berlin Beamforming Conference, 29 February-1 March 2016*, February 2016.

[8] S. Oerlemans and P. Sijtsma. Determination of Absolute Levels from Phased Array Measurements Using Spatial Source Coherence. In *8th AIAA/CEAS Aeroacoustics Conference and Exhibit, Breckenridge, Colorado, June 17-19, 2002*, 2002.

[9] Sijtsma P. Clean based on spatial source coherence. *International Journal of Aeroacoustics*, 6(4):357–374, December 2007.

[10] Thomas Padois and Alain Berry. Two and three-dimensional sound source localization with beamforming and several deconvolution techniques. *Acta Acustica united with Acustica*, 103(3):392–400, may 2017.

[11] Thomas Padois, Philippe-Aubert Gauthier, and Alain Berry. Inverse problem with beamforming regularization matrix applied to sound source localization in closed wind-tunnel using microphone array. *Journal of Sound and Vibration*, 333(25):6858–6868, 2014.

[12] A. Pereira, J. Antoni, and Q. Leclère. Empirical bayesian regularization of the inverse acoustic problem. *Applied Acoustics*, 97:11–29, oct 2015.

[13] Antonio Pereira. *Acoustic imaging in enclosed spaces*. PhD thesis, INSA de Lyon, 2014.

[14] E. Sarradj. Three-dimensional acoustic source mapping with different beamforming steering vector formulations. *Advances in Acoustics and Vibration*, 2012(292695):1–12, 2012.

[15] Takao Suzuki. L1 generalized inverse beam-forming algorithm resolving coherent/incoherent, distributed and multipole sources. *Journal of Sound and Vibration*, 330:5835–5851, 2011.

[16] A. N. Tikhonov. Solution of incorrectly formulated problems and the regularization method. *Soviet Math. Dokl.*, 4:1035–1038, 1963.